



LAWRENCE
LIVERMORE
NATIONAL
LABORATORY

Computational Study of the Energetics and Defect-Clustering Tendencies for Y and La-doped UO₂

B. Sadigh, J. Solomon, V. Alexandrov, A.
Navrotsky, M. Asta

January 29, 2014

Acta Materialia

Disclaimer

This document was prepared as an account of work sponsored by an agency of the United States government. Neither the United States government nor Lawrence Livermore National Security, LLC, nor any of their employees makes any warranty, expressed or implied, or assumes any legal liability or responsibility for the accuracy, completeness, or usefulness of any information, apparatus, product, or process disclosed, or represents that its use would not infringe privately owned rights. Reference herein to any specific commercial product, process, or service by trade name, trademark, manufacturer, or otherwise does not necessarily constitute or imply its endorsement, recommendation, or favoring by the United States government or Lawrence Livermore National Security, LLC. The views and opinions of authors expressed herein do not necessarily state or reflect those of the United States government or Lawrence Livermore National Security, LLC, and shall not be used for advertising or product endorsement purposes.

Computational Study of the Energetics and Defect-Clustering Tendencies for Y and La-doped UO₂

J.M. Solomon^{a,*}, V. Alexandrov^b, B. Sadigh^c, A. Navrotsky^{d,e}, M. Asta^{a,d,e}

^a*Department of Materials Science and Engineering, University of California, Berkeley, CA 94720, USA*

^b*Physical Sciences Division, Pacific Northwest National Laboratory, Richland, Washington 99352, USA*

^c*Physical and Life Science Directorate, Lawrence Livermore National Laboratory, Livermore, California, 94550, USA*

^d*Peter A. Rock Thermochemistry Laboratory and NEAT ORU, University of California, Davis, California 95616, USA*

^e*Department of Chemical Engineering and Materials Science, University of California, Davis, California 95616, USA*

Abstract

The energetics and defect-ordering tendencies in solid solutions of fluorite-structured UO₂ with trivalent rare earth cations (M³⁺=Y, La) are investigated computationally using a combination of ionic-pair-potential and density-functional-theory (DFT) based methods. Calculated enthalpies of formation with respect to constituent oxides show higher energetic stability for La solid solutions relative to Y, consistent with the differences in experimentally measured solubility limits for the two systems. Additionally, calculations performed for different atomic configurations show a preference for reduced (increased) oxygen vacancy coordination around La (Y) dopants. The current results are shown to be qualitatively consistent with related calculations and calorimetry measurements in other trivalent-doped fluorite-structured oxides, which show a tendency for increasing stability and increasing preference for higher oxygen coordination with increasing size of the trivalent impurity. The implications of these results are discussed in the context of the effect of trivalent impurities on oxygen-ion mobilities in UO₂, which are relevant to the understanding of experimental observations concerning the effect of trivalent fission products on oxidative corrosion rates of spent nuclear fuel.

*Corresponding author. email: jsolom@berkeley.edu

Keywords: oxygen vacancy, formation enthalpy, pyrochlore, DFT

1. Introduction

Fluorite-structured oxide compounds can often be doped with high concentrations of trivalent cations. Under reducing conditions this doping leads to the formation of charge-compensating oxygen vacancy defects. Recent calorimetry studies on trivalent-cation doped ZrO_2 [1], HfO_2 [2], CeO_2 [3] and ThO_2 [4] provide evidence for strong defect association in such systems. The experimental findings have been shown to be consistent with recent first principles computational work on some of these same systems, which demonstrate energetic binding/clustering tendencies between cations and oxygen vacancies, to a degree that has been found to correlate strongly with ionic radii [5, 6, 7, 8, 9, 10, 11, 12]. Strong oxygen vacancy-cation association is known to reduce the mobility of oxygen ions and therefore the ionic conductivity in aliovalently-doped fluorite-structured oxides, which can be detrimental for their use in fuel cell electrolyte and oxygen sensor applications [13].

Similar effects have also been discussed in the context of the electrochemical behavior of spent nuclear fuel composed of fluorite-structured UO_2 with soluble trivalent fission products. Specifically, recent studies have attributed rare earth (i.e., trivalent) fission product dopant-oxygen vacancy clusters to the decreased rate of oxidative dissolution with increasing burnup in spent fuel [14]. The defect clusters are believed to reduce the concentration of mobile oxygen vacancies which facilitate oxidation and eventual dissolution of the fuel, in a similar manner that rare earth doping impedes air oxidation of the cubic fluorite structure to orthorhombic U_3O_8 [15, 16, 17, 18]. Oxidation and dissolution of nuclear fuel in aqueous environments is of particular concern at the back end of the fuel cycle, i.e., waste disposal [19, 20].

Because of the significant changes in oxidation and corrosion behavior of nuclear fuel associated with rare earth fission products, understanding the thermochemical properties of these defects in UO_2 is of particular interest. The effect of rare earth fission product doping on the oxygen chemical potential in UO_2 has been studied extensively [21]. However, the understanding of the energetics and defect-ordering tendencies of these systems remains less advanced compared to other fluorite-structured oxides (see Refs. [5, 6, 7, 8, 9, 10, 11, 12]). Specifically, only one calorimetry study [22] and

one ionic pair-potential modeling investigation [23] have been reported to date. The aim of the current work is to provide further insight into the thermochemical behavior of UO_2 doped with trivalent cations through the application of density-functional-theory (DFT) based calculations in which we explore stability and defect ordering/clustering trends with respect to relative cation sizes. It is widely accepted that UO_2 substituted with trivalent cations will contain oxygen vacancies or localized electron holes (i.e., U^{5+}) as charge-compensating defects. The current work focuses only on systems with oxygen vacancies. We consider the smallest and largest trivalent rare earth fission product cations that are soluble in UO_2 , namely, Y^{3+} (1.02 Å ionic radius with eightfold coordination) and La^{3+} (1.16 Å) [24].

The remainder of the paper is organized as follows. In the next section the details of the calculations are described, and are followed by a presentation of the results for formation energetics and defect interactions in Section 3. In Section 4 the results are discussed in the context of the previous models proposed for explaining the effect of cation size on the stability and defect-ordering behavior in aliovalently doped fluorite structures.

2. Computational Methodology

The computational approach employed in this work is similar to that applied in studies of doped ZrO_2 and ThO_2 by Bogicevic *et al.* [8, 9] and Alexandrov *et al.* [11], respectively. The approach involves calculations of a relatively large number of ordered defect-dopant configurations as a basis for exploring trends in energetic stability and defect ordering. The following subsections provide detailed descriptions of the structural enumeration techniques (Sec. 2.1), the screening of the structures using ionic pair-potential models (Sec. 2.2), and the DFT-based calculations (Sec. 2.3) implemented in this work.

2.1. Structure Enumeration

In order to determine the most stable defect structures for fluorite-structured UO_2 doped with trivalent cation (M^{3+}) oxides, we investigate many hypothetical cation vacancy arrangements. The fluorite-based cation sublattice contains host and dopant species (i.e., U^{4+} and M^{3+} , respectively), and the anion sublattice contains host and vacancy species (i.e., O^{2-} and O_{vac}), respectively (the substitution of two U^{4+} by M^{3+} can be charge-compensated by one O_{vac}), as illustrated in Fig. 1. We employ a structure enumeration

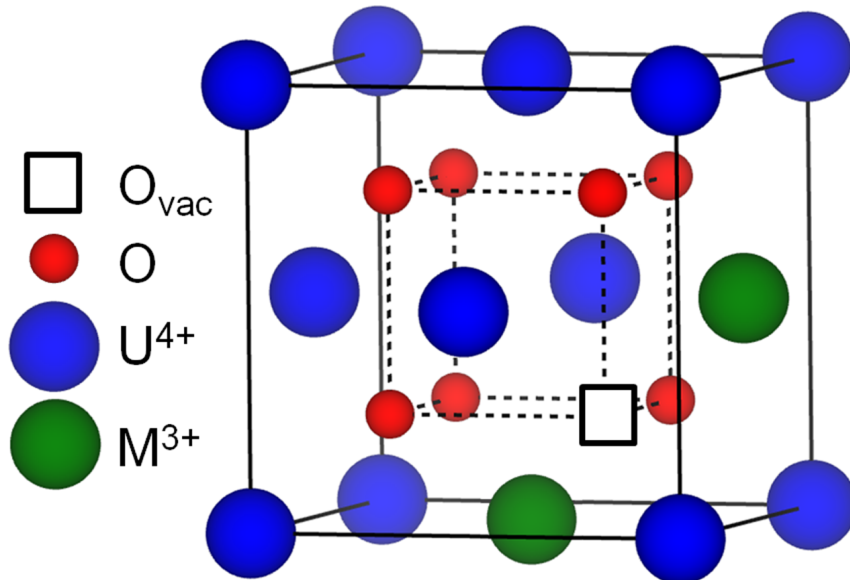


Figure 1: The ideal UO_2 cubic fluorite structure with two trivalent dopants on the cation fcc sublattice and one charge-compensating oxygen vacancy on an anion simple cubic sublattice is shown.

technique developed for cluster-expansion-based studies of alloy thermodynamics, considering supercells consisting of up to six formula units, employing an algorithm by Hart and Forcade [25] that is implemented in the alloy theoretic automatic toolkit (ATAT) [26, 27]. The compositions considered are $\text{U}_4\text{M}_2\text{O}_{11}$ ($x=1/3$, six formula units: 4 U ions, 2 M ions, 11 O ions, and 1 O_{vac}), $\text{U}_2\text{M}_2\text{O}_7$ ($x=1/2$, four formula units: 2 U ions, 2 M ions, 7 O ions, and 1 O_{vac}), and $\text{U}_2\text{M}_4\text{O}_{10}$ ($x=2/3$, six formula units: 2 U ions, 4 M ions, 10 O ions, and 2 O_{vac}). The structure enumeration yielded 117, 27, and 710 symmetry-distinct structures for $x=1/3$, $1/2$, and $2/3$, respectively.

2.2. Classical Pair Potentials

The energies of all enumerated structures were calculated using ionic pair-potential models as a first “screening” step, with the intent of eliminating from consideration by more computationally demanding DFT-based calculations the electrostatically-unfavorable structures for a given composition and M^{3+} species. The potential energy between ions i and j is expressed

mathematically as

$$E(r_{ij}) = \frac{q_i q_j}{r_{ij}} + A \exp\left(\frac{-r_{ij}}{\rho}\right) - \frac{C}{r_{ij}^6} \quad (1)$$

The first term represents the coulombic interaction where q is the respective ionic charge and r_{ij} is the distance between ions i and j . The latter two repulsive and attractive terms represent the short range Buckingham potential, where A , ρ , and C are system-dependent parameters. In addition, polarizabilities were introduced for individual ionic species according to the shell model as formulated by Dick and Overhauser [28]. The Buckingham and shell model parameters used in this work are given in Refs. [29, 30, 31]. Geometry relaxations and energy minimizations were performed using the General Utility Lattice Program [32].

2.3. First-principles Calculations

All structures for a given composition and M^{3+} species were ranked according to their total energy based on the ionic pair potential calculations described in the previous section. Initially DFT calculations were performed for the resulting six lowest-energy structures for a given composition. If any of the five higher-energy structures were found to be lower than the ground state predicted by the pair potential models, additional structures were considered in an effort to ensure that the lowest-energy configuration was identified by the DFT-based methods.

Most of the results reported below were obtained using DFT within the formalism of the projector augmented-wave (PAW) method [33, 34] and the Perdew-Burke-Ernzerhof (PBE) generalized gradient approximation (GGA) [35, 36] as implemented in the Vienna *ab initio* simulation package (VASP) [37, 38]. Additionally, a Hubbard-U correction was implemented within the formalism of Dudarev *et al.* [39] to account for the self-interaction error for localized $5f$ electrons in uranium. The value of the parameter $U_{eff} = U - J$ in the DFT+U formalism was chosen to be 4.00 eV for this study; this value is similar to that found to give optimal results in comparisons to spectroscopic data by Dudarev *et al.* (3.99 eV) [39], which has been used extensively in the literature, and was found to provide good agreement between calculated and measured oxidation enthalpies of UO_2 [40]. The PAW potentials used in this work are U, O, Y_sv, and La in the VASP PBE library. The PAW potentials use 14 valence electrons for U ($6s^2 6p^6 5f^3 6d^1 7s^2$), 6 for O

($2s^22p^4$), 11 for Y ($4s^24p^65s^24d^1$), and 11 for La ($5s^25p^66s^25d^1$). We employ a plane-wave cutoff energy of 500 eV, and the Brillouin zone is sampled using the Monkhorst-Pack scheme with at least $4 \times 4 \times 4$ k-point meshes. Atomic positions were relaxed with no symmetry constraints until residual forces were below approximately 20 meV/Å. From convergence checks with respect to plane-wave cutoff and k-point sampling we estimate the formation enthalpies to be converged at the level of a few tenths of a kJ/mol-cation. The results of the first-principles calculations presented below made use of a scalar-relativistic approximation. We also performed calculations of the lowest energy Y and La-substituted structures for $x=1/2$ including spin-orbit coupling, which was found to change the formation enthalpies by a magnitude of less than 1 kJ/mol-cation.

The formation enthalpy for a solid solution with respect to its constituent oxides is defined as

$$\Delta H_f = E[U_{1-x}M_xO_{2-0.5x}] - (1-x)E[UO_2] - xE[MO_{1.5}], \quad (2)$$

where $E[U_{1-x}M_xO_{2-0.5x}]$ denotes the energy per cation of a solid solution with cation dopant concentration x , $E[UO_2]$ denotes the energy per cation of fluorite-structured UO_2 (calculated here using a 12-atom unit cell with 1k antiferromagnetic order), and $E[MO_{1.5}]$ denotes the energy per cation of Y_2O_3 or La_2O_3 in the experimentally observed (i.e., room temperature) cubic bixbyite (C-type sesquioxide) or hexagonal (A-type) structure, respectively. Both ferromagnetic and antiferromagnetic arrangements for the uranium ion local magnetic moments were considered within the solid solution defect structures, and the latter was found to be lower in energy. Because there are four uranium atoms in the structures associated with $x=1/3$, there are three unique antiferromagnetic spin arrangements (i.e., up-up-down-down, up-down-up-down, up-down-down-up). We found little difference in the calculated formation enthalpies with respect to each of these magnetic configurations (i.e., within 0.2 kJ/mol-cation).

In calculations that make use of the DFT+U methodology, it is well documented in the literature that one can converge to multiple metastable states corresponding to different orbital occupancies for the localized f electrons. Thus, a practical issue in such calculations is to ensure that the computed energy corresponds to the true electronic ground state (or close to it) [41, 42]. Several different methods have been proposed to address this issue for UO_2 [43, 44, 45, 46, 47]. In this work we employ the approach by Meredig *et al.*

[47], involving a gradual “ramping” up of the Hubbard-U parameter. In the current implementation, U_{eff} starts at zero and is increased stepwise by 0.1 eV in order to localize the U 5*f* electrons. This methodology offers sufficient computational efficiency for treating many compounds with relatively large unit cells.

In order to be confident of the accuracy of the “U-ramping” method, we compared results obtained by this approach with those derived by the occupation matrix control (OMC) method, which has been applied to plutonium oxides (PuO₂ and Pu₂O₃) [48] and subsequently UO₂ [45, 46]. The OMC approach involves initializing calculations with many distinct imposed values of the diagonal and off-diagonal occupation matrices for the U 5*f* electrons, and taking the lowest of the resulting calculated energies as the ground-state.

For comparison of the “U-ramping” and OMC methods we performed static DFT+U calculations of a simple defect-fluorite structure, namely, ULa₂O₅, which contains a single oxygen vacancy. We used the OMC approach discussed in Ref. [45] in which a total of 61 occupation matrices were sampled (21 diagonal, 40 off-diagonal). The ramping method gave the lowest total energy by approximately 2.4 kJ/mol-cation compared the lowest total energy determined using OMC. A more exhaustive sampling of matrices in the OMC approach could potentially result in energies that are closer to (or perhaps even lower) than resulting from the “U-ramping” approach; however, it is encouraging that none of the energies derived from the OMC method were significantly lower than that obtained from the ramping approach.

Separate DFT calculations using a hybrid functional [49] were implemented to compare results to formation enthalpies calculated using the DFT+U method. The hybrid functional methodology has been shown to accurately describe lattice constants and electronic structure of UO₂ [50, 51, 52, 53, 54]. The “local hybrid functional for correlated electrons” (LHFCE), which is also referred to as “exact exchange for correlated electrons” (EECE), is a hybrid functional in which the exact exchange is applied locally within the atomic spheres only to the correlated electrons (i.e., 5*f* in the current work). The LHFCE functional is less computationally demanding compared to the full hybrid functional, and has been shown to accurately describe lattice constants, electronic structure, and defect formation energies of UO₂ [55, 56].

The LHFCE calculations were performed using the all-electron full-potential linearized augmented plane wave plus local orbitals basis (FP-L/APW+lo) method as implemented in the WIEN2k code. Details of the LHFCE method implementation in WIEN2k are discussed in Ref. [57]. The hybrid exchange-

correlation energy functional used in this work has the form

$$\Delta E_{XC}^{PBE+\alpha HF} = \alpha E_X^{HF} + (1 - \alpha) E_X^{PBE} + E_C^{PBE}, \quad (3)$$

where αE_X^{HF} is the HF exchange, E_X^{PBE} and E_C^{PBE} are the PBE exchange and correlation energies, respectively, and α represents the fraction of HF exchange that replaces the PBE exchange. The value for α used in this work is 0.25, which is representative of the PBE0 functional [58].

In the FP-L/APW+lo method the convergence of the basis set is controlled by a cutoff parameter $R_{rmt}K_{max}$, where R_{rmt} is the smallest atomic sphere radius in the cell and K_{max} is the magnitude of the largest wavenumber of the plane wave expansion. Additional local orbitals were added for U 6s, 6p, 4d, 5f and for O 2s states. The R_{rmt} values were set to 2.3 Bohr, 1.6 Bohr, 2.26 Bohr, and 2.3 Bohr for U, O, Y, and La, respectively, and $R_{rmt}K_{max} = 8$. The Brillouin zone was sampled with 32 k-points and the integrations were conducted by the tetrahedron method of Blöchl, Jepsen, and Andersen [33]. The spin-polarized calculations were performed with antiferromagnetic configurations for the structures containing uranium atoms. The energy, charge, and force convergence criteria used for these computations are 1 meV, 0.0001 and 26 meV/Å.

3. Results

The results for all calculations presented below were computed using the GGA+U method, unless explicitly stated otherwise. We first investigate the energetic stability of $U_{1-x}M_xO_{2-0.5x}$ (M=Y,La) through consideration of the formation enthalpy ΔH_f with respect to constituent oxides, as defined in Eq. 2. Results for the lowest energy structures of Y and La-substituted UO_2 are shown in Fig. 2 and Table 1. The positive values of ΔH_f for Y-containing solid solutions indicate that phase separation is favored at low temperatures, whereas the negative values of ΔH_f for La-containing solid solutions indicate a compound forming tendency.

The formation enthalpy values for calculations with the hybrid functional are consistent with the DFT+U calculations for both Y and La-substituted systems, with respect to the order of magnitude and sign of ΔH_f , and the trend with substitution level, as shown in Fig. 2. A comparison of the filled and open symbols, corresponding respectively to GGA+U and hybrid-functional results, show agreement at the level of a few kJ/mol-cation. This

Table 1: Formation enthalpies of $U_{1-x}M_xO_{2-0.5x}$ (M=Y,La) structures are listed for low-energy fully relaxed structures enumerated in this study. The structures listed have formation energies within 3 kJ/mol-cation of the lowest energy structure for each trivalent cation species at each composition considered. The fourth column lists the direction of ordering of oxygen vacancies. The last column lists the number of trivalent cations in the four tetrahedral nearest-neighbor positions surrounding an oxygen vacancy.

x	M	ΔH_f	Direction	# M-Vac Neighbors
2/3	La	-1.6	$\langle 110 \rangle$	2
		10.8	$\langle 110 \rangle$	3
	Y	11.3	$\langle 211 \rangle$	3
		12.3	$\langle 211 \rangle$	3
		12.6	$\langle 211 \rangle$	3
		12.6	$\langle 110 \rangle$	3
1/2	La	-1.3	$\langle 110 \rangle$	1
		1.4	$\langle 110 \rangle$	1
		2.1	$\langle 110 \rangle$	1
	Y	11.5	$\langle 110 \rangle$	3
1/3	La	-5.2	$\langle 211 \rangle$	0
		7.5	$\langle 211 \rangle$	2
		8.3	$\langle 211 \rangle$	2
		8.9	$\langle 211 \rangle$	2
		9.2	$\langle 110 \rangle$	3

good level of agreement between calculated results obtained using different codes and functionals is encouraging. Additionally, the trend that Y solid solutions are less energetically stable than La systems, obtained with both the DFT+U and hybrid calculations, is consistent with experimentally measured solubility limits which are higher for the latter: 83 mol % La at 1250°C in $\text{UO}_2\text{-La}_2\text{O}_3$ versus 48 mol % Y at 2000°C in $\text{UO}_2\text{-Y}_2\text{O}_3$ [59, 60]; specifically, the formation enthalpy is indicative of the magnitude of the excess free energy, and more positive ΔH_f values are expected to have lower solubility limits.

We consider next the relative ordering of the cation/vacancy configurations giving the lowest formation enthalpies. Table 1 lists, for the most stable configurations, the formation enthalpy and structural features including the direction of oxygen vacancy ordering and the number of trivalent cations (per vacancy site) that are nearest-neighbors to an oxygen vacancy (for structures with $x=2/3$ that contain two oxygen vacancies, the reported number of nearest-neighbor cations is an average over both vacancy sites). In the fluorite lattice, each oxygen vacancy has four cation nearest neighbors, therefore the maximum number of M^{3+} nearest-neighbors to the vacancy site is four. We observe that the oxygen vacancies prefer to align as either second or sixth nearest neighbors along the $\langle 110 \rangle$ and $\langle 112 \rangle$ directions, respectively. In the lowest-energy structures for Y-substituted systems, a higher number of M^{3+} neighbors around the vacancies are preferred compared to the La-substituted systems for all compositions.

The formation enthalpies for all structures computed by the GGA+U method in this study are shown in Fig. 3. The wide range of enthalpies for each composition illustrates the magnitude of the dependence of the energy on the defect configuration. Y-substituted systems for $x=1/3$ and $2/3$ show several nearly-degenerate low energy structures, whereas the lowest-energy configuration for La-substituted systems shows a larger gap between the lowest and next-lowest energy structures for all three compositions. The results in Fig. 3 again highlight the stronger energetic preference for M^{3+} binding with oxygen vacancies in the Y- versus La-substituted systems.

4. Discussion

To gain additional insights into the factors governing the stability of trivalent impurities in UO_2 , we compare below the main results of the present work with those derived in previous computational and experimental studies

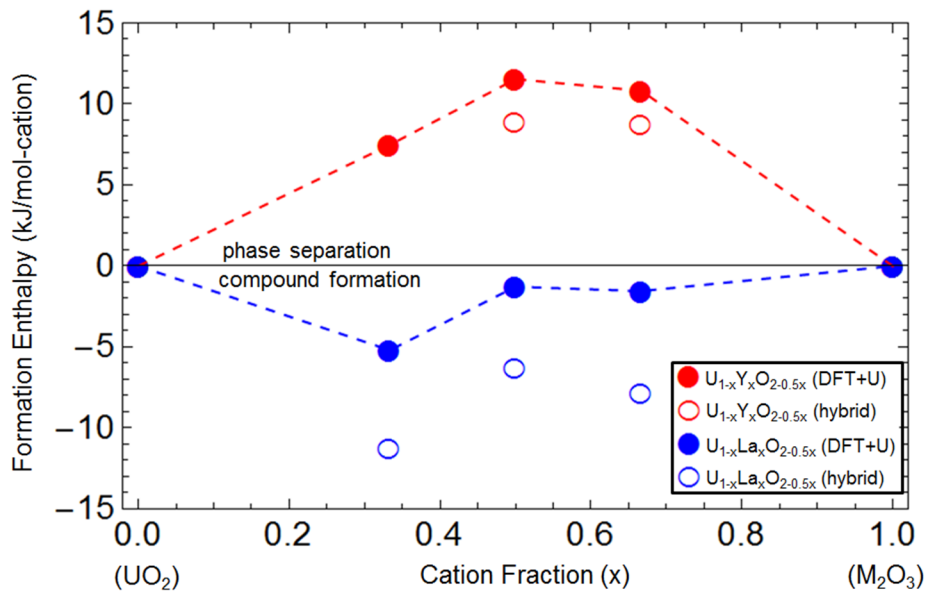


Figure 2: Formation enthalpies of $U_{1-x}M_xO_{2-0.5x}$ ($M=Y,La$) structures are shown for the lowest-energy fully relaxed structures of all compositions enumerated in this study.

of the energetics of aliovalently-doped fluorite-structured oxide solid solutions [11, 8, 3, 4]. The present results for UO_2 are shown to be consistent with previously reported trends concerning the effect of cation size on the formation energies of other trivalent-doped fluorite-structured oxide solid-solutions. Additionally, the nature and energetics of cation-vacancy ordering derived from the present results are analyzed, and the consequences of these findings for oxygen-ion mobilities are discussed.

4.1. Energetic Trends with Host Cation

For a given trivalent impurity (Y^{3+} or La^{3+}) the formation enthalpies presented above for UO_2 -based solid solutions are lower than those computed in a previous DFT study of ThO_2 -based systems [11]. Specifically, we obtain negative formation enthalpies for all compositions for La-substituted UO_2 , whereas ΔH_f was found to be positive for La substitutions in ThO_2 in previous GGA calculations [11] and calorimetry measurements [4]. Similarly, the positive formation energies plotted in Fig. 2 for Y-doped UO_2 are smaller in magnitude than those reported previously for Y-doped ThO_2 [11]. Considering that the ionic radius of U^{4+} (1.00 Å) is smaller than that of Th^{4+} (1.05 Å), these comparisons suggest a trend towards higher energetic stability (lower

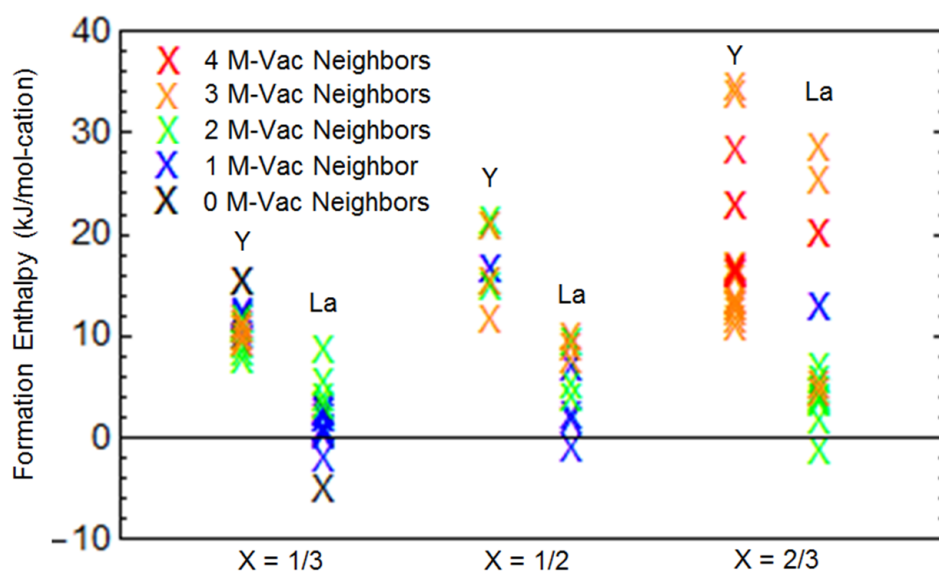


Figure 3: The formation enthalpies calculated using DFT+U for all structures computed in this study are shown. Each structure is denoted by the number of trivalent cations in the four tetrahedral nearest-neighbor positions surrounding an oxygen vacancy according to the legend in the top left of the figure. Note that there are two vacancy sites for $x=2/3$, and the average number of neighbors between the two sites (rounded to the nearest neighbor) is shown.

formation energies) with decreasing size of the 4+ host cation, for a given M^{3+} impurity. This trend is also observed if the present calculated values of ΔH_f for Y-doped UO_2 are compared with those derived in previous DFT calculations for Y-doped ZrO_2 [8]; the latter are found to be significantly lower in energy, consistent with the smaller ionic radius of Zr^{4+} (0.84 Å).

The effect of the 4+ cation size is summarized for Y-doped solid solutions in Fig. 4 (similar behavior is also found for La-doping, although fewer results are available in the literature). The data plotted in Fig. 4 displays a clear trend towards increasing stability (decreasing enthalpy) with decreasing radius of the 4+ cation. This trend is consistent with observations derived from calorimetry experiments by Chen and Navrotsky [3] and Aizenshtein, Shvareva and Navrotsky [4]. In an analysis of the measured formation enthalpies across trivalent-doped ThO_2 , CeO_2 , ZrO_2 and HfO_2 , these authors have argued that the enhanced stability of systems with smaller 4+ cations is associated with a preference for reduced oxygen-ion coordination. Specifically, the formation of a fluorite-structured solid solution from AO_2 and M_2O_3 constituents necessarily leads to a decrease in the average oxygen coordination surrounding the A^{4+} cation, relative to the eightfold coordination characteristic of the pure AO_2 constituent. For small cations such as Zr^{4+} and Hf^{4+} , which are known to prefer sevenfold coordination, this effect is expected to be stabilizing. More generally, for a fixed trivalent impurity, the decrease in oxygen coordination around the A^{4+} host cation resulting from solid-solution formation is expected to be increasingly energetically favorable with decreasing A^{4+} ionic radius.

4.2. Energetic Trends with Trivalent Cation

We consider next the trends in ΔH_f with respect to the size of the trivalent cation, for a fixed 4+ cation species. In Fig. 2, UO_2 solid solutions with the larger La trivalent ions are shown to be more stable energetically (i.e., feature lower values of ΔH_f) relative to those with the smaller Y ions. This trend towards more positive formation energies for Y versus La trivalent dopants is consistent with both calorimetry and computational results in CeO_2 and ThO_2 systems [3, 4, 11].

To explore this trend further we consider the relative energy of $U_{0.5}La_{0.5}O_{1.75}$ and $U_{0.5}Y_{0.5}O_{1.75}$ compounds with two different structures: (i) the most stable Y-substituted structure with $x=1/2$, and (ii) the most stable La-substituted structure with $x=1/2$. For structure (i) we find that the La-containing compound has a formation enthalpy that is 4.1 kJ/mol-cation

lower than that for the Y-containing compound, and for structure (ii) the formation enthalpy is lower for the La-containing compound by 12.8 kJ/mol-cation. For both structures the La-containing compound features a lower formation energy, by an amount that depends on the exact nature of the cation-vacancy arrangement (for a discussion of the effect of cation and vacancy ordering see subsection Sec. 4.3).

It has been suggested [3, 4] that the trend towards increasing ΔH_f with decreasing size of the trivalent cation can be attributed to the smaller lattice distortions that have been observed to occur when larger trivalent cations are substituted into oxygen-vacancy charge-compensated fluorite-structured oxide compounds. Specifically, molecular dynamics simulations of La- and Y-substituted CeO₂ show much smaller changes in the nearest-neighbor cation-cation nearest-neighbor distances for La- relative to Y-substituted structures [61]. We find similar trends in the present work: La-U and U-U distances in U_{0.5}La_{0.5}O_{1.75} structures are computed to be at most 0.08 Å different from the nearest-neighbor spacing on the cation sublattice of pure UO₂, while for U_{0.5}Y_{0.5}O_{1.75} structures these bond-length distortions (i.e., Y-U, U-U) are as large as 0.20 Å.

4.3. Nature of Cation-Vacancy Ordering

We turn now to an analysis of the nature of the energetically-favorable cation-vacancy ordering tendencies for the UO₂-M₂O₃ structures considered in this work. We consider first the lowest-energy structure of composition U₂La₂O₇ (x= 1/2), which is computed to have a negative formation enthalpy in the present study, suggesting a tendency towards stable compound formation. We focus on this particular stoichiometry, as it is characteristic of the pyrochlore structure (A₂B₂O₇) which is found to be a thermodynamically stable compound for many systems [62]. The pyrochlore structure is a derivative of fluorite where the A and B cations are ordered along the $\langle 110 \rangle$ direction, and the tetrahedrally-coordinated oxygen vacancies are surrounded by adjacent A⁴⁺ cations. The configuration of the pyrochlore structure requires eight formula units (4 U ions, 4 La ions, 14 O ions, and 2 *O_{vac}*), and was therefore not considered in our structure enumerations, which considered compounds with four formula units for x=1/2. However, we performed an additional calculation of the formation enthalpy for pyrochlore-structured U₂La₂O₇, obtaining a value of $\Delta H_f = +5.8$ kJ/mol-cation, which is roughly 7 kJ/mol-cation higher in energy than the lowest-energy configuration for ΔH_f identified in this work. The relatively high energy of the pyrochlore

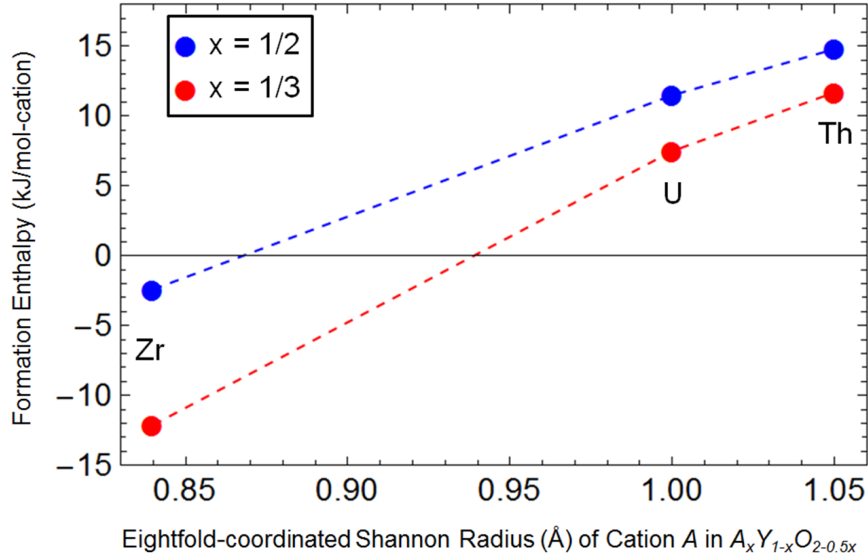


Figure 4: Calculated formation enthalpies for Y-substituted fluorite systems are shown. Results for zirconia (A=Zr) and thoria (A=Th) systems were taken from Refs. [8] and [11], respectively.

structure for this system is consistent with arguments suggested previously based on the B^{3+}/A^{4+} cation size ratios required for pyrochlore stability [62]. Specifically, a characteristic of the pyrochlore structure is that the oxygen vacancies are entirely surrounded by tetravalent cations (i.e., A^{4+}), and the A^{4+} cation must be sufficiently small relative to the B^{3+} cation such that the oxygen coordination is not energetically too unfavorable. According to Ref. [62], pyrochlore structures are stable if the B^{3+}/A^{4+} radius ratio is between 1.46-1.80, where the B^{3+} radius is for the trivalent cation with eightfold coordination, and the A^{4+} radius is that for the tetravalent cation with sixfold coordination. The ratio for $U_2La_2O_7$ is 1.30, which is consistent with lack of stability of the pyrochlore compound for this system.

To gain insight into the nature of the preferred interactions between the trivalent dopants and charge-compensating oxygen vacancies in UO_2 - M_2O_3 solid solutions, we plot in Fig. 5 formation enthalpies for three structures featuring different number of trivalent-cation/oxygen-vacancy nearest neighbors, for both $M=La$ and Y . The three structures considered have the same vacancy ordering pattern (i.e., $\langle 110 \rangle$) and one, two or three M^{3+} -vacancy neighbors. The configurations chosen are 1) the lowest-energy Y-substituted

structure (three M^{3+} - O_{vac} neighbors), 2) the lowest-energy La substituted structure (one M^{3+} - O_{vac} neighbor), and 3) a structure with two M^{3+} -vacancy neighbors that is within 4 kJ/mol-cation of the lowest energy structure for both La and Y-substituted systems. The results in Fig. 5 demonstrate that Y and La dopants display qualitatively different preferences; the formation enthalpies for Y- and La- substituted structures increase and decrease, respectively, with respect to the number of M^{3+} -vacancy neighbors.

The different signs of the slopes in Fig. 5 for the Y- and La- substituted structures can be understood qualitatively based on the the size of the trivalent cations. Specifically, as discussed in Sec. 4.1, we expect that the the larger La cations would prefer higher oxygen ion coordination relative to Y cations. This trend is consistent with the results in Fig. 3, which show that the lowest energy structure for La-containing solid solutions generally feature fewer neighbors with oxygen vacancies compared to Y-containing structures. This trend is also consistent with the simulation results from Refs. [7, 63], which show that fluorite systems doped with larger trivalent dopant cations prefer to have the oxygen vacancies at distances from the trivalent impurity that are farther from the nearest-neighbor coordination shell, in part due to relaxation effects that outweigh the coulombic attraction between the effectively positively charged oxygen vacancy and negatively charged M^{3+} cation.

For Y- and La- containing solid solutions, the results in Fig. 5 suggest a significant energetic preference for M^{3+} -oxygen vacancy and U^{4+} -oxygen vacancy clustering, respectively. In both cases, these clustering tendencies would be expected to lower oxygen-ion mobility, as discussed previously in the context of ionic conductivity in fluorite-structured solid electrolytes [13]. The current results thus support the suggestion from Ref. [14] that the effect of increased burnup (leading to higher concentrations of soluble trivalent fission products) on oxidative corrosion rates in spent nuclear fuel can be attributed to lower oxygen mobility due to defect association.

5. Conclusions

In this study DFT-based computational methods were employed to study formation energetics and defect-ordering tendencies in UO_2 compounds substituted with Y and La cations, which are common soluble fission products in nuclear fuel. We consider substitutional configurations that are charge-compensated with oxygen vacancies, finding that phase separation is energet-

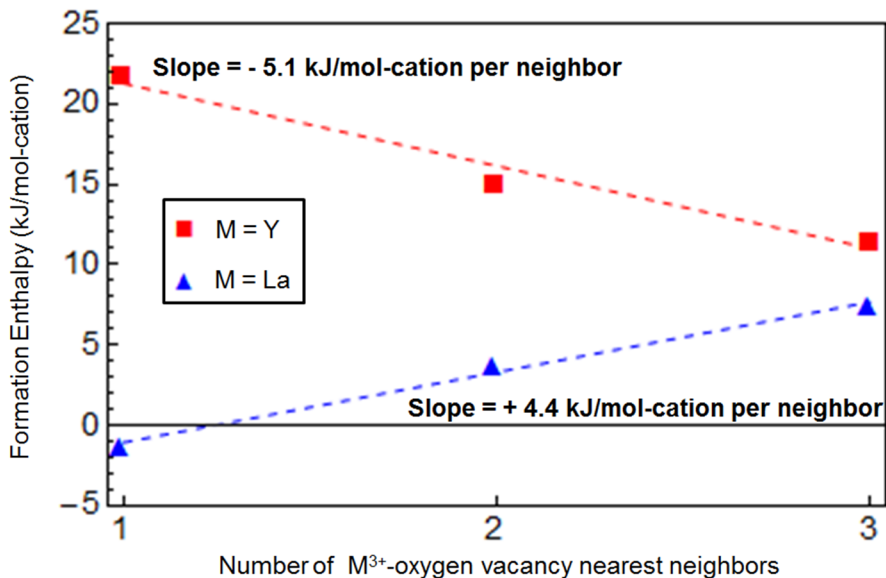


Figure 5: The formation enthalpies for selected structures containing, one, two, and three trivalent cation nearest neighbors to an oxygen vacancy are shown for Y and La-substituted systems at $x=1/2$.

ically favored for all compositions considered for Y-substituted UO_2 , whereas compound formation is favored for La-substituted UO_2 . The calculations are thus characterized by a trend towards increasing energetic stability of solid solutions with the larger La impurity relative to the smaller Y impurity. This trend is consistent with previous computational and calorimetric studies [3, 4, 11] for fluorite-structured solid solutions based on CeO_2 and ThO_2 .

We observe in general that oxygen vacancies prefer to align as either second or sixth nearest neighbors on the oxygen sublattice along the $\langle 110 \rangle$ and $\langle 112 \rangle$ directions, respectively, suggesting that the energetically preferred defect-ordering configurations are characterized by a repulsive interaction between nearest-neighbor oxygen vacancies. In the Y-substituted systems, structures with an enhanced number of vacancies around the Y^{3+} ions are found to be favored energetically, while the opposite is found for La-substituted systems. The pronounced energetic preferences for dopant-vacancy or host-cation-vacancy clustering are expected to have an important effect on oxygen-ion mobilities and therefore the oxidative corrosion rates in spent nuclear fuel.

6. Acknowledgments

J.M. Solomon was supported by the Office of Basic Energy Sciences of the U.S. Department of Energy as part of the Materials Science of Actinides Energy Frontier Research Center (DE-SC0001089) for initial DFT+U calculations, U.S. Department of Energy by Lawrence Livermore National Laboratory (DE-AC52-07NA27344) for the hybrid calculations, and the Department of Defense through the National Defense Science & Engineering Graduate Fellowship Program for the remainder of the work. V. Alexandrov, A. Navrotsky, and M. Asta were supported by the U.S. Department of Energy as part of the Materials Science of Actinides Energy Frontier Research Center (DE-SC0001089). B. Sadigh was supported by Department of Energy by Lawrence Livermore National Laboratory (DE-AC52-07NA27344). This work made use of resources of the National Energy Research Scientific Computing Center, supported by the Office of Basic Energy Sciences of the U.S. Dept of Energy (DE-AC02-05CH11231). The authors would like to thank B. E. Hanken and L. Zhang for useful discussions.

References

- [1] T. A. Lee, A. Navrotsky, I. Molodetsky, *Journal of Materials Research* 18 (2003) 908–918.
- [2] T. A. Lee, A. Navrotsky, *Journal of Materials Research* 19 (2004) 1855–1861.
- [3] W. Chen, A. Navrotsky, *Journal of Materials Research* 21 (2006) 3242–3251.
- [4] M. Aizenshtein, T. Y. Shvareva, A. Navrotsky, *Journal of the American Ceramic Society* 93 (2010) 4142–4147.
- [5] A. K. A. Pryde, S. Vyas, R. W. Grimes, J. A. Gardner, R. Wang, *Phys. Rev. B* 52 (1995) 13214–13222.
- [6] M. S. Khan, M. S. Islam, D. R. Bates, *J. Mater. Chem.* 8 (1998) 2299–2307.
- [7] L. Minervini, M. O. Zacate, R. W. Grimes, *Solid State Ionics* 116 (1999) 339 – 349.

- [8] A. Bogicevic, C. Wolverton, G. M. Crosbie, E. B. Stechel, *Phys. Rev. B* 64 (2001) 014106.
- [9] A. Bogicevic, C. Wolverton, *Phys. Rev. B* 67 (2003) 024106.
- [10] A. Predith, G. Ceder, C. Wolverton, K. Persson, T. Mueller, *Phys. Rev. B* 77 (2008) 144104.
- [11] V. Alexandrov, N. Grønbech-Jensen, A. Navrotsky, M. Asta, *Phys. Rev. B* 82 (2010) 174115.
- [12] M. O. Zacate, L. Minervini, D. J. Bradfield, R. W. Grimes, K. E. Sickafus, *Solid State Ionics* 128 (2000) 243 – 254.
- [13] H. Inaba, H. Tagawa, *Solid State Ionics* 83 (1996) 1 – 16.
- [14] H. He, P. G. Keech, M. E. Broczkowski, J. J. Nol, D. W. Shoesmith, *Canadian Journal of Chemistry* 85 (2007) 702–713.
- [15] L. Thomas, R. Einziger, H. Buchanan, *Journal of Nuclear Materials* 201 (1993) 310 – 319.
- [16] J.-W. Choi, R. J. McEachern, P. Taylor, D. D. Wood, *Journal of Nuclear Materials* 230 (1996) 250 – 258.
- [17] J. Cobos, D. Papaioannou, J. Spino, M. Coquerelle, *Journal of Alloys and Compounds* 271273 (1998) 610 – 615.
- [18] R. McEachern, P. Taylor, *Journal of Nuclear Materials* 254 (1998) 87 – 121.
- [19] M. E. Torrero, E. Baraj, J. de Pablo, J. Gimnez, I. Casas, *International Journal of Chemical Kinetics* 29 (1997) 261–267.
- [20] D. Shoesmith, *Journal of Nuclear Materials* 282 (2000) 1 – 31.
- [21] D. Shin, T. M. Besmann, *Journal of Nuclear Materials* 433 (2013) 227 – 232. And references therein.
- [22] L. Mazeina, A. Navrotsky, M. Greenblatt, *Journal of Nuclear Materials* 373 (2008) 39 – 43.

- [23] S. Middleburgh, D. Parfitt, R. Grimes, B. Dorado, M. Bertolus, P. Blair, L. Hallstadius, K. Backman, *Journal of Nuclear Materials* 420 (2012) 258 – 261.
- [24] R. D. Shannon, *Acta Crystallographica Section A* 32 (1976) 751–767.
- [25] G. L. W. Hart, R. W. Forcade, *Phys. Rev. B* 77 (2008) 224115.
- [26] A. van de Walle, M. Asta, G. Ceder, *Calphad* 26 (2002) 539 – 553.
- [27] A. van de Walle, *Calphad* 33 (2009) 266 – 278.
- [28] B. G. Dick, A. W. Overhauser, *Phys. Rev.* 112 (1958) 90–103.
- [29] D. J. Binks, R. W. Grimes, *Journal of the American Ceramic Society* 76 (1993) 2370–2372.
- [30] G. Busker, A. Chroneos, R. W. Grimes, I.-W. Chen, *Journal of the American Ceramic Society* 82 (1999) 1553–1559.
- [31] R. W. Grimes, G. Busker, M. A. McCoy, A. Chroneos, J. A. Kilner, S. P. Chen, *Berichte der Bunsengesellschaft für physikalische Chemie* 101 (1997) 1204–1210.
- [32] J. D. Gale, A. L. Rohl, *Molecular Simulation* 29 (2003) 291–341.
- [33] P. E. Blöchl, *Phys. Rev. B* 50 (1994) 17953–17979.
- [34] G. Kresse, D. Joubert, *Phys. Rev. B* 59 (1999) 1758–1775.
- [35] J. P. Perdew, K. Burke, M. Ernzerhof, *Phys. Rev. Lett.* 77 (1996) 3865–3868.
- [36] J. P. Perdew, K. Burke, M. Ernzerhof, *Phys. Rev. Lett.* 78 (1997) 1396–1396.
- [37] G. Kresse, J. Furthmüller, *Phys. Rev. B* 54 (1996) 11169–11186.
- [38] G. Kresse, J. Furthmüller, *Computational Materials Science* 6 (1996) 15 – 50.
- [39] S. L. Dudarev, G. A. Botton, S. Y. Savrasov, C. J. Humphreys, A. P. Sutton, *Phys. Rev. B* 57 (1998) 1505–1509.

- [40] B. E. Hanken, C. R. Stanek, N. Grønbech-Jensen, M. Asta, *Phys. Rev. B* 84 (2011) 085131.
- [41] A. Shick, W. Pickett, A. Liechtenstein, *Journal of Electron Spectroscopy and Related Phenomena* 114116 (2001) 753 – 758.
- [42] P. Larson, W. R. L. Lambrecht, A. Chantis, M. van Schilfgaarde, *Phys. Rev. B* 75 (2007) 045114.
- [43] H. Y. Geng, Y. Chen, Y. Kaneta, M. Kinoshita, Q. Wu, *Phys. Rev. B* 82 (2010) 094106.
- [44] F. Zhou, V. Ozoliņš, *Phys. Rev. B* 83 (2011) 085106.
- [45] B. Dorado, B. Amadon, M. Freyss, M. Bertolus, *Phys. Rev. B* 79 (2009) 235125.
- [46] B. Dorado, G. Jomard, M. Freyss, M. Bertolus, *Phys. Rev. B* 82 (2010) 035114.
- [47] B. Meredig, A. Thompson, H. A. Hansen, C. Wolverton, A. van de Walle, *Phys. Rev. B* 82 (2010) 195128.
- [48] G. Jomard, B. Amadon, F. m. c. Bottin, M. Torrent, *Phys. Rev. B* 78 (2008) 075125.
- [49] A. D. Becke, 98 (1993) 5648–5652.
- [50] K. N. Kudin, G. E. Scuseria, R. L. Martin, *Phys. Rev. Lett.* 89 (2002) 266402.
- [51] I. D. Prodan, G. E. Scuseria, R. L. Martin, *Phys. Rev. B* 73 (2006) 045104.
- [52] L. E. Roy, T. Durakiewicz, R. L. Martin, J. E. Peralta, G. E. Scuseria, C. G. Olson, J. J. Joyce, E. Guziewicz, *Journal of Computational Chemistry* 29 (2008) 2288–2294.
- [53] X.-D. Wen, R. L. Martin, L. E. Roy, G. E. Scuseria, S. P. Rudin, E. R. Batista, T. M. McCleskey, B. L. Scott, E. Bauer, J. J. Joyce, T. Durakiewicz, *Journal of Chemical Physics* 137 (2012) 154707.

- [54] X.-D. Wen, R. L. Martin, G. E. Scuseria, S. P. Rudin, E. R. Batista, *The Journal of Physical Chemistry C* 117 (2013) 13122–13128.
- [55] F. Jollet, G. Jomard, B. Amadon, J. P. Crocombette, D. Torumba, *Phys. Rev. B* 80 (2009) 235109.
- [56] J.-P. Crocombette, D. Torumba, A. Chartier, *Phys. Rev. B* 83 (2011) 184107.
- [57] P. Novak, J. Kune, L. Chaput, W. E. Pickett, *Physica Status Solidi (b)* 243 (2006) 563–572.
- [58] C. Adamo, V. Barone, *The Journal of Chemical Physics* 110 (1999).
- [59] E. Stadlbauer, U. Wichmann, U. Lott, C. Keller, *Journal of Solid State Chemistry* 10 (1974) 341 – 350.
- [60] S. F. Bartram, E. F. Juenke, E. A. Aitken, *Journal of the American Ceramic Society* 47 (1964) 171–175.
- [61] H. Hayashi, R. Sagawa, H. Inaba, K. Kawamura, *Solid State Ionics* 131 (2000) 281 – 290.
- [62] M. Subramanian, G. Aravamudan, G. S. Rao, *Progress in Solid State Chemistry* 15 (1983) 55 – 143.
- [63] M. O. Zacate, L. Minervini, D. J. Bradfield, R. W. Grimes, K. E. Sickafus, *Solid State Ionics* 128 (2000) 243 – 254.